The Effect of Noise on Reverberation-Chamber Measurements of Antenna Efficiency

The Effect of Noise on Reverberation-Chamber Measurements of Antenna Efficiency

Anouk Hubrechsen, *Student Member, IEEE*, Kate A. Remley, *Fellow, IEEE*, Robert D. Jones, *Student Member, IEEE*, Dylan F. Williams, *Fellow, IEEE*, Dazhen Gu, *Senior Member, IEEE*, Adrianus B. Smolders, *Senior Member, IEEE*, and Laurens A. Bronckers, *Member, IEEE*

***Abstract*—In this work, we show that high antenna frequency selectivity can make it more challenging to accurately measure antenna efficiency in a reverberation chamber when using the two-antenna method, since electronic noise can affect the measured stirred-energy component of the S-parameters. Recognizing whether the measured antenna-efficiency estimate is significantly affected by electronic noise is not trivial. The measured S-parameters used for calculation may have high SNRs, but the antenna-efficiency estimate can still show large systematic errors due to noise. We model noise as a component of the measured stirred energy, showing that the measured reflection is much more susceptible to noise than the measured transmission. We do not focus on the origin of the noise, but rather on the effect it has on the measurement. We show the effect of noise on the overestimation of the stirred energy components of the S-parameters, which affects the two-antenna formulation more significantly than the three-antenna method one. We show that this overestimation can cause efficiency estimates calculated with the two- and three-antenna methods to be significantly over- or under-estimated and we show that uncertainties increase as well. Finally, we provide clear steps to recognize and reduce noise effects in antenna efficiency measurements.**

***Index Terms*—Antenna efficiency, Internet-of-things, Microwave measurement, Noise, Reverberation chambers, Uncertainty, Wireless system**

I. Introduction

5G-and-beyond requirements are pushing for new technological innovations to meet societal demands such as ubiquitous coverage, increased reconfigurability, and mobility. A significant part of meeting these demands in 5G communications will be through Internet-of-Things (IoT) or machine-to-machine (M2M) applications, which will largely operate in the sub-6 GHz bands (400 MHz - 6 GHz) [1]–[5]. Such mobile 5G devices can introduce new antenna designs, such as narrowband antennas that are tunable over frequency, operating in multiple bands, or those with high rejection bands in-between [6]–[19]. Characterizing such small and low-cost devices is challenging, since their antennas can have high internal antenna losses or they can be highly mismatched for certain bands within their operational frequency range. These devices are expected to be often used in highly reflective, scattering environments [4]–[6], making antenna efficiency more important than other metrics such as directivity.

Antenna efficiency can be characterized both in an anechoic chamber (AC) [20]–[24] and a reverberation chamber (RC) [25]–[33]. The RC approach for characterizing antenna efficiency has gained popularity in recent years due to the flexibility of device placement in the test volume and rapid, low-cost measurements. These characteristics are much desired for measuring future mobile devices, since they generally have a short development time and may have unusual form factors.

Multiple techniques have been proposed to determine antenna efficiency in an RC, both with and without a dependence on a reference antenna with a known efficiency. Popular methods that do not depend on the use of a reference antenna with a known efficiency are the one-, two-, and three-antenna methods [32]. They are based on the difference in the RC's quality factor (Q) as computed in the frequency and time domains, where the latter does not include the early-time behavior of the RC or the antenna efficiency [34], [35]. The former does, so this difference between the two can be directly related to antenna efficiency. The two-antenna method is a preferable technique for determining antenna characteristics, since it relies on fewer assumptions than the one-antenna method, but it takes approximately, depending on instrumentation settings, less than half the measurement time as compared to the three-antenna method. This leads to a fast, hence, low-cost measurement that does not hamper development time.

It has been shown that the two- and three-antenna methods can provide accurate results for high-efficiency and broadband antennas [32], [36], [37]. However, as we will show, large systematic errors in efficiency can occur when the two-antenna method is used with highly-mismatched or high-loss antennas such as a narrowband antenna with a high rejection band. An example is presented in Fig. 1. This figure shows a large discrepancy in the total efficiency of a broadband horn estimated with the two-antenna method when the second antenna is narrowband. This is compared to a two-antenna method case where the second antenna is a broadband antenna, or compared to a three-antenna method case where the second antenna is narrowband and the third is broadband. As we will show, these errors can be especially hard to notice because the reflection-coefficient measurement used to derive the two-antenna result

A. Hubrechsen was with the National Institute of Standards and Technology (NIST), Boulder, CO 80305 USA. She is now with the Electrical Engineering department of the Eindhoven University of Technology, 5612 AZ Eindhoven, The Netherlands. (e-mail: a.hubrechsen@tue.nl).

K. A. Remley, R. D. Jones, D. F. Williams and D. Gu are with the National Institute of Standards and Technology (NIST), Boulder, CO 80305 USA (e-mail: kate.remley@nist.gov, robert.jones@nist.gov, dazhen.gu@nist.gov, dylan.williams@nist.gov).

A. B. Smolders and L. A. Bronckers are with the Electrical Engineering department of the Eindhoven University of Technology, 5612 AZ Eindhoven, The Netherlands. (e-mail: a.b.smolders@tue.nl, l.a.bronckers@tue.nl).

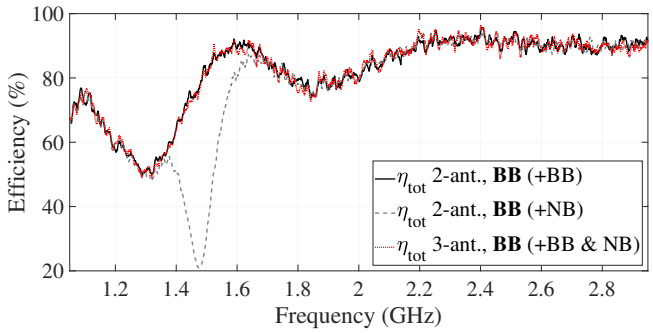

Fig. 1. Total efficiency of a broadband (BB) antenna, measured with the two- and three-antenna methods, with a narrowband (NB) and/or a BB antenna as a second and/or third antenna. The two-antenna method total-efficiency estimate calculated with a NB antenna shows large discrepancies with the three-antenna method estimate, or the two-antenna estimate calculated with a BB antenna.

may have a high SNR, even though electronic noise can still cause a systematic error in the efficiency results. Due to the increasing popularity of this method, it is necessary that these effects are investigated in detail. To the authors' knowledge, only one earlier work has reported a similar observation with the one- and two-antenna methods, but the origin of this effect was not investigated in that work [31].

For the first time, we will illustrate a dependency on noise with an extensive study on the effects of noise on the two- and three-antenna methods, where we mainly focus on the two-antenna method. Note that this work does not contain an analysis on the types of noise influencing the measurements, as they are likely a combination of many different types of noise (e.g. thermal, shot, phase, regeneration and recombination noise), so we refer to the combination as 'electronic noise'. However, this assumption does not significantly change the main noise effects presented in this work since, regardless of its physical origins, a noise signal in a frequency band of interest may be modeled as a random variable in the mathematical sense [38]. We refer the reader to [39] for a more extensive noise analysis. In Section II, we describe the currently reported accuracy constraints and provide three use cases to show that there is an additional noise constraint associated with these methods. In Section III, we introduce noise as a component of the measured stirred energy. In Section IV, we show the impact of noise as a component in the measured stirred energy on antenna efficiency for multiple use cases, including a more robust approach to estimate uncertainty for antenna efficiency. In Section V, we discuss how to recognize and reduce the noise effects. The work is concluded in Section VI.

II. Constraints on Antenna-Efficiency Methodologies

We describe the currently known constraints and assumptions of the one-, two-, and three-antenna methods to show that the current constraints are not limited to the type of antenna used. Then we provide different use cases with different antenna types with low total efficiencies, to show experimentally that there is a previously unreported additional constraint related to noise.

A. One-, Two- and Three-Antenna Methods Constraints

In this work, we mainly focus on total efficiency. In [32], total antenna efficiency is defined by the ratio between the power radiated by the antenna and the power available at the antenna port. Radiation efficiency is defined by the ratio between the power radiated by the antenna and the power accepted by the antenna port, as defined in [40]. The three-antenna method can be directly derived from fundamental reverberation-chamber theory as shown in [41]. Since the technique is derived from equations that assume an unloaded (or very lightly loaded) chamber, the currently known limitations of this method are based on the assumption that *the losses in the RC are dominated by the chamber walls*. This implies the following assumptions:

1) The antenna-efficiency measurements should ideally be performed in a chamber that is not heavily loaded [42]. The antennas used in this work do not increase the chamber loading significantly and, therefore, the antenna choice is not limited by this constraint.
2) It can become problematic to determine the chamber decay time, τ_{RC}, as required in the three-antenna method when losses (due to chamber loading or internal antenna losses) become high, due to the short late-time measurement time interval [31], [32], [43], [44]. In such a case, fewer data samples are used in the calculation of τ_{RC}, increasing uncertainty in the estimate of antenna efficiency. In a three-antenna case, this constraint can be easily avoided by using the transmission coefficient of two low-loss antennas in the calculation, as we do in this work.

The one- and two-antenna methods can be derived from the three-antenna method by introducing an enhanced backscattering constant (e_b), defined as the ratio between the stirred components of the reflection and the transmission coefficients, see Fig. 2 [45]. The assumptions on this constant in the one- and two-antenna methods are [32]:

1) In the two-antenna method, e_b is assumed to not change over position, orientation and polarization in the chamber.
2) The one-antenna method assumes $e_b = 2$, which only holds for an ideal, well-stirred chamber.

In RC measurements, the enhanced backscatter constant usually deviates slightly from $e_b = 2$, and it has been shown that e_b can vary over position and polarization [46]. Therefore, the two-antenna method can be less accurate than the three-antenna method. Nevertheless, these assumptions do not place any constraints on the type or performance of the antenna. Thus, if the time-constant constraint is avoided, the one-, two- and three-antenna methods could be expected to work for all antenna types. Note that this is clearly not the case as shown in Fig. 1. In fact, the two-antenna method has an additional, previously unpublished, constraint related to noise. We will show that this constraint relates to the stirred energy component being susceptible to noise. Next, we develop experiments with different antennas, to show that the effect of Fig. 1 is not specific to that antenna used.

B. Use Cases

We study three use cases in this work. In the first use case, we focus on the narrowband antenna that caused the discrepancy seen in Fig. 1. This antenna is a frequency-reconfigurable antenna that shows both high mismatch and high internal antenna loss within the band of interest. To separate these effects, we introduce two more use cases: Use Case 2, to study antenna-mismatch effects (high radiation efficiency), and Use Case 3, for internal antenna-loss effects (low radiation efficiency). We estimate the total antenna efficiency using both the two- and three-antenna methods for all cases. For an extensive explanation of these methods, we refer the reader to [32]. The use cases, as also shown in Table 1, are:

1) Frequency-reconfigurable antenna (FRA): This antenna uses voltages applied to Barium Strontium Titanate (BST) capacitors as a tuning mechanism [6]. These capacitors absorb most of the energy for frequencies just above the input match, leading to a rejection band adjacent to the receiving band. Therefore, this antenna has high internal losses and is narrowband (less than 20 MHz -10 dB bandwidth). This antenna is an example of a typical antenna that could be used in future handheld devices. In this case, we configured the antenna to be matched at 1.4 GHz.
2) Discone antenna cascaded with a 50 MHz bandpass filter (DAF), with the -3dB passband between 1420 and 1470 MHz: This mimics a narrowband antenna that is designed to have both a passband and a rejection band. The rejection band is caused by a band filters' out-of-band response (mismatch effect). Such an antenna with both a passband and a rejection band is another typical example of a future mobile device. The discone antenna used was a Bluetest C disone[1], operating band 0.65-3.5 GHz.
3) Discone antenna cascaded with a 50 dB attenuator (DAA): This acts as an antenna designed to have a large rejection band, caused by internal losses of the antenna. The discone antenna used was the same as the one used in Use Case 2.

Throughout the paper we will refer to these three use cases. All measurements shown are performed in the 1 GHz - 3 GHz frequency range, since the frequency-reconfigurable antenna in Use Case 1 is reconfigurable within this frequency range. For the sake of brevity, we only show one tuning setting, but similar noise effects were observed for other settings.[2] We use a discone antenna in Use Case 2 and 3 because we expect it has similar far-field behavior as the frequency-reconfigurable antenna of Use Case 1. The second and third antenna in all use cases, as presented in Table I, are dual-ridge horn antennas (DRHA1 and DRHA2), both ETS model 3115[1], which were used as reference antennas for the two- and three-antenna methods since they have low internal antenna loss and low mismatch effects, and a high directivity which can yield a better K-factor.

[1]We use trade names only to completely explain the experimental conditions. This does not constitute an endorsement by NIST. Other products may work as well or better.

[2]The same effect was observed in 30 measurements, where the antenna was tuned in steps of 100 MHz in the 1 - 3 GHz band.

TABLE I
ANTENNAS USED IN USE CASES 1-3

Use Case	Antenna 1	Antenna 2	Antenna 3
1	FRA	DRHA1	DRHA2
2	DAF	DRHA1	DRHA2
3	DAA	DRHA1	DRHA2

III. NOISE IN STIRRED ENERGY

A key component to understanding the discrepancy in Fig. 1, is the dependency of each method on different scattering parameters (S-parameters). All methods use chamber decay time, frequency and chamber volume. Otherwise, the three-antenna method depends only on measured transmission parameters, unlike the one- and two-antenna methods, which depend on measured reflection parameters as well. A dependency on the measured reflection parameters can be undesirable, because it can have reduced contributions to the stirred-energy component from the mode-strirring mechanisms, compared to the measured transmission coefficient, as we will show. In this section, we describe the process used to obtain the stirred-energy component, and we introduce a new description that includes noise.

All S-parameter measurements that are performed in an RC consist of stirred and unstirred-energy components, as illustrated in Fig. 2 for S-parameters related to Antenna 1 [41], [47]. Stirred energy has a low correlation between every stepped mode-stirring sample, while unstirred energy introduces correlation into the measurement. Additionally, any measured S-parameter will also contain a third component, which is a noise component.

In antenna-efficiency measurements, it is common practice to obtain an estimate of the stirred-energy component by removing the unstirred energy in post processing [32]. For a given mode-stirring sample n, this process is given by

$$S^n_{ij,s} = S^n_{ij} - \langle S_{ij} \rangle_N, \tag{1}$$

where $S_{ij,s}$ and $\langle S_{ij} \rangle$ are the stirred and unstirred-energy component estimate of S_{ij}, respectively, and i and j are the port indices of the vector network analyzer (VNA) and where i can be equal to j. N is the number of mode-stirring samples. Note that the unstirred-energy component is generally much higher for $i = j$, since a large part of the unstirred-energy component consists of the reflection coefficient of the antenna, whereas only unstirred energy from chamber effects contributes to the unstirred-energy component when $i \neq j$ (see Fig. 2). The stirred-energy component contains the efficiencies of the antennas in the RC, but it also contains noise. We can extract the antenna efficiency by using chamber constants and $\langle |S_{ij,s}|^2 \rangle$, the variance of S^n_{ij}.

The variance consists of contributions from the different stepped-paddle positions which can be modeled as a random variable. The paddle contributions are not truly random because the variation in the RC channel is deterministic and repeatable from one measurement to the next. However, the variation of samples taken over paddle positions is modeled as random since it has a complex Gaussian distribution (Rayleigh in magnitude) [41]. Electronic noise from the measurement

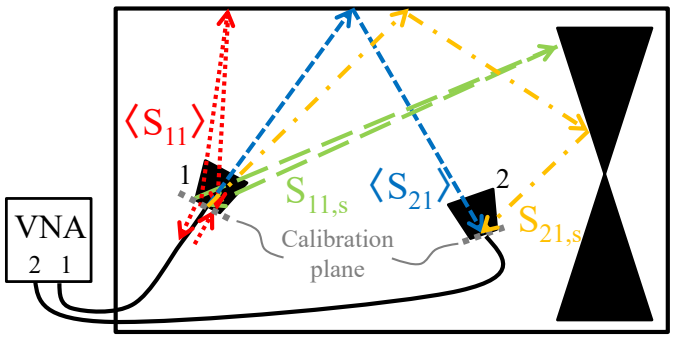

Fig. 2. Illustration of the stirred and unstirred components of the S-parameters related to antenna 1. Note that $S_{11,s}$ is attenuated twice by the total efficiency of Antenna 1 compared to $S_{21,s}$, making it more susceptible to noise if this efficiency is low. $\langle S_{11}\rangle$ contains the reflection coefficient of Antenna 1 as well. This is not the case for $\langle S_{21}\rangle$, so for a well-stirred chamber $\langle S_{11}\rangle$ is generally much larger than $\langle S_{21}\rangle$.

setup, including instrumentation, will be a zero-mean random variable as well (see [39]) and hence, contributes to the variance, especially for low received signals as occurs in antennas with a low total efficiency. Thus, the variance of S_{ij} to the first-order of approximation can be written as a combination of contributions from the paddles and the noise as

$$\langle |S_{ij,s}|^2\rangle = \langle |S_{ij,\text{paddles}} + S_{ij,\text{noise}}|^2\rangle_N, \tag{2}$$

where $S_{ij,\text{noise}}$ and $S_{ij,\text{paddles}}$ are the zero-mean contributions to the stirred energy by the noise and the mode-stirring mechanisms (here abbreviated as 'paddles'), respectively. Including a dependency on noise in these equations is key to understanding the susceptibility to noise of these antenna-efficiency methods, as the relation between the paddle and noise contributions directly relates to the signal-to-noise ratio (SNR). We refer the reader to [39] for an extensive analysis of the probability distributions of the noise in general S-parameter VNA measurements.

For high-total-efficiency antennas, the contribution of the noise to $\langle |S_{ii,s}|^2\rangle$ and $\langle |S_{ij,s}|^2\rangle$ is negligible compared to the contribution of the paddles. However for high-antenna-loss or highly-mismatched antennas (low total efficiency), this may not be the case, as the contribution of the mode-stirred energy can be less than that of the noise. As can be derived from (2), this increased relative contribution of the noise can lead to an overestimated variance of the S-parameter, which consequentially leads to an over- or under-estimated efficiency (Eq. 27 in [32]). Inherently, this effect becomes more significant in the measured S_{ii} of a low-total-efficiency antenna (given a second high-total-efficiency antenna), assuming $\langle |S_{ii,\text{noise}}|^2\rangle \approx \langle |S_{ij,\text{noise}}|^2\rangle$. In such a case, the waves contributing to the mode-stirred energy ($S_{ii,\text{paddles}}$) experience twice the attenuation of the low-total efficiency antenna (round trip) compared to only once for transmission parameters (single trip), as illustrated in Fig. 2. Since the one- and two-antenna methods use S-parameters where $i = j$, they are more susceptible to noise effects than the three-antenna method, which only uses S-parameters where $i \neq j$. Note that this effect is hard to distinguish from regular reverberation-chamber behavior. The measured S_{ii} is usually well above the noise floor, while its stirred energy component may be below the noise floor. Especially when one does not know the efficiency of an antenna, this effect can remain unnoticed. Next, we show the impact of the overestimation of the variances on the antenna-efficiency estimates of all use cases and we show its contribution to the uncertainties.

IV. Noise Impact on Antenna Efficiency

In this section, we illustrate the systematic error caused by the overestimation of parameters due to noise. We also determine the measurement uncertainty due to both systematic and random effects in order to judge the significance of the noise effect on our estimate of total efficiency. First, we describe our method for estimating the uncertainty for total efficiency. Then, we show the experiment setup and present the results for total efficiency for each use case.

A. Measurement Uncertainty

We show an extended approach for estimating uncertainty in antenna-efficiency measurements. We used a similar approach as presented for the two-antenna method in [48] that takes into account uncertainties due to both systematic and random effects. Due to the non-linearity of the operators used in the efficiency equations, the method uses a Monte Carlo approach. The uncertainty estimates were calculated using the National Institute of Standards and Technology (NIST) Microwave Uncertainty Framework (MUF) [49], which is an open-source framework to process measurement uncertainties including correlations between components of uncertainty. The algorithms included in the MUF that we used are extensively explained in [50]–[54]. We refer the reader to a more extensive explanation of the specific method used in this work to [48]. We extend this existing method in three ways:

1) We extend the existing approach for estimating uncertainty due to unknown errors in the VNA calibration standard dimensions to the three-antenna method. Since we cannot perform a full-wave measurement [55], because our VNA had only three samplers, we make three two-port measurements for every mode-stirring sample and combine them afterwards.
2) We refer to the uncertainties due to random effects, estimated from independent relations, as "uncertainty due to independent realization differences" instead of "uncertainty due to lack of spatial uniformity," since we do not expect the lack of spatial uniformity to be the main source of uncertainty, nor is the random component due to an insufficient number of mode-stirring samples. As we will show, independent realizations can differ significantly due to small variations in the unstirred component becoming significant.
3) To obtain the combined uncertainty, we combine the uncertainties due to systematic effects from one independent realization of the stirring sequence with uncertainties due to random effects, determined from all independent realizations. This saves time, but also preserves the probability density functions throughout the entire procedure

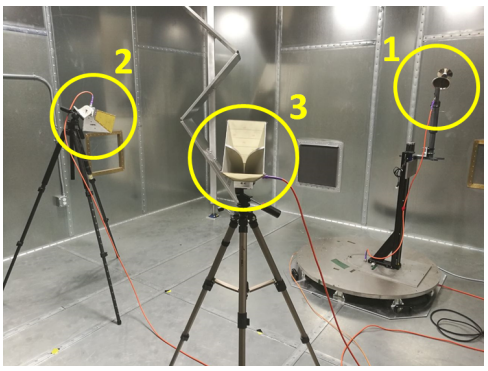

Fig. 3. Setup in the NIST RC for Use Case 3, showing Antennas 1-3. Due to the height of the chamber, the horizontal paddle is not visible in this picture, but it is situated on the top left.

and takes correlations into account, unlike the root-sum-squared (RSS) technique used in [48].

For all efficiency results shown in this work, we report the 2σ deviation of the combined uncertainty from the mean, that is, 95 % confidence interval including a coverage factor [54].

B. Experiment Setup

We performed all measurements in this work in an RC located at NIST, with dimensions 4.74 x 4.13 x 5.18 m^3, as shown in Fig. 3. The RC has one horizontal paddle and one vertical paddle for mechanical mode stirring, and a turntable to obtain independent realizations. Antenna 1 (see Table I) was placed on the turntable, and Antennas 2 and 3 were stationary. We obtained 12 independent realizations of the mode-stirring sequence, obtained by measuring at different antenna positions, since typically, a minimum of $P = 9$ independent realizations are required [42]. Each independent realization contained 100 mode-stirring samples (10 paddle positions for both the vertical and horizontal stirrer), verifying low correlation by ensuring an autocorrelation with a threshold of 0.6 (2σ). Even though all samples are never truly independent, we use the term independent samples for samples with a correlation below this threshold. We used a three-sampler VNA with an IF BW of 1 kHz, 100 kHz frequency spacing, 10 μs dwell time and -8 dBm stimulus power. For these settings, the SNR of the VNA was approximately 100 dB. The calibration reference plane was located at the connectors of the antennas and we calibrated the VNA with an N-type electronic calibration module.

From these measurements, we use the average of all independent realizations to obtain the total-efficiency estimate. We calculate total efficiency for the three use cases we presented in Section II with both the two- and three- antenna methods, according to the configurations presented in Table I. We measured all S-parameters between the three VNA ports for every use case, where VNA ports 1, 2 and 3 were connected to the Antennas 1, 2 and 3, as presented in Table 1, respectively. From three two-port measurements over a single mode-stirring sequence, we then estimated the total efficiency of all antennas with both the two- and three-antenna methods. To minimize uncertainty in the chamber-decay time, we extract τ_{RC} from the transmission between Antennas 2 and 3 as they have low losses. In post-processing, we frequency-averaged the results using a 100 MHz averaging bandwidth.

To compare results, we illustrate the noise error effect on the total-efficiency estimate of DRHA1 (Antenna 2), as this antenna is used in all use cases for both the two- and three-antenna methods (See Table I). As described earlier, an overestimation of $S_{11,s}$ causes the same total-efficiency overestimation in Antenna 1, as it causes an underestimation in Antenna 2. Therefore, studying the effects on Antenna 2 is sufficient to represent the errors and uncertainties. As a reference for the total efficiency of DRHA1, we used a three-antenna method efficiency estimate obtained from a measurement with all high-total-efficiency and broadband antennas. The three-antenna method was used as a reference since this method can be directly related back to fundamental theory and it has been shown to work for high-total-efficiency and broadband antennas [37]. For each case of determining total efficiency, we judge that there is a discrepancy between the use case and the reference when the confidence intervals of the estimate and the reference do not overlap.

C. Antenna-Efficiency Results

Fig. 4(a-c) show Use Case 1-3, in which FRA, DAF, or DAA are used, respectively, to estimate the total efficiency of DRHA1 for different methods and antenna configurations. We show the measured efficiency of the (a) FRA, (b) DAF and (c) DAA as well for reference (note that the efficiency of the DAA is nearly zero due to its 50 dB attenuation). For every use case, the only configuration that shows discrepancies is a configuration where the two-antenna method is used with a low-total-efficiency antenna. Also, these discrepancies appear in different frequency bands, and with different uncertainties, as we discuss next.

1) Discrepancies: First, we focus on the discrepancies between the two-antenna method and other methods shown in Fig. 4, which are caused by systematic errors due to noise. The low total efficiency of Antenna 1 at certain frequencies (including the operating band) causes a low SNR of the stirred parameter at those frequencies, so the noise contribution becomes significant and $S_{11,s}$ is overestimated. Consequently, the efficiency of DRHA1 is underestimated in these cases, and the efficiency of Antenna 1 is overestimated. Note that the magnitude of the discrepancy is not directly proportional to the total efficiency of Antenna 1 over frequency, since the noise variance varies over frequency, which both affect the SNR. To quantify the systematic error, these results show discrepancies from the reference of up to approximately 10 dB (maximum errors at 1.45 GHz in Fig.4(a), 2.6 GHz in (b) and 2.2 GHz in (c)) but it should be noted that this is highly dependent on the chamber configuration and experiment setup.

2) Uncertainties: Second, we focus on the uncertainties shown in Fig. 4. The reported error bars correspond to a 95% confidence interval. Note that we do not report a full uncertainty analysis, but we focus on the most significant contributors [48]. In each measurement, the uncertainty due to

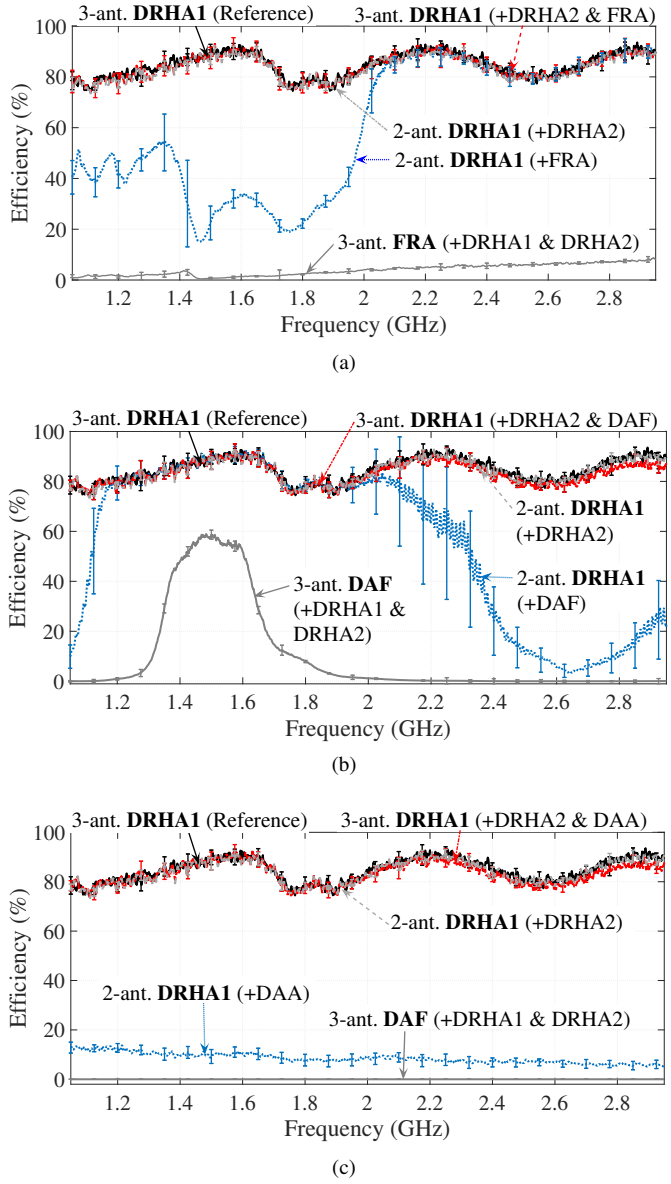

Fig. 4. Total efficiency of DRHA1 (Antenna 2) for Use Cases 1, 2 and 3, shown in (a), (b), and (c), respectively. The total efficiency of Antenna 1 of each use case was included for reference. For cases where Antenna 1 was used to calculate the two-antenna method efficiency estimate, the efficiency of DRHA1 showed significant underestimations due to an overestimation of $S_{11,s}$, and increased uncertainties due to the ratio between a large unstirred and a small stirred component.

unknown errors in the VNA calibration standard dimensions was below 0.1 dB over the complete frequency band. In the reference measurement, the uncertainty due to independent realization differences was below 0.2 dB. Note that the uncertainty may significantly vary within the frequency band, as shown in Fig. 4.

For the two-antenna method cases that show significant discrepancies, uncertainties due to differences between independent realizations are much higher than in the reference measurement. For example, as shown in Fig. 4(a), the uncertainty was approximately 0.1 dB above 2.2 GHz, but increased significantly around 1.4 GHz, where this uncertainty component was approximately 3.0 dB. Note that in this case, the large uncertainty occurred within the operating band, due to a low total efficiency. This same range of uncertainty over frequency occurred in Fig. 4(b), but now in the rejection band. In (c), this range was approximately 1.1 dB to 2.0 dB, as the noise effect is significant in the complete band.

The increased uncertainty in efficiency was mainly due to an increased uncertainty in $\langle|S_{11,s}|^2\rangle$, which showed large deviations over different turntable positions, or independent realizations. The increased uncertainty is caused by two effects. First, since $\langle|S_{11,s}|^2\rangle$ mainly consists of noise for very low total efficiencies, a small change in noise variance over position can become significant. Second, since the RC is not ideal, the measured unstirred component, $\langle S_{11}\rangle$, can change slightly over position. This is usually negligible, but this can become significant when the stirred component is much smaller, for example for antennas with low total efficiencies, as can be derived from (1). This effect is higher for antennas with a high mismatch as compared to those with a high internal antenna loss, because the former causes a much higher unstirred component (due to a higher reflection coefficient). Therefore, uncertainties are higher in Fig. 4(a) and (b) as compared to Fig. 4(c). Since the other antennas had a high total efficiency, all other S-parameter variances in these measurements did not show this effect. We only focus on total efficiency in this work, but note that radiation efficiency has an extra dependency on $\langle S_{11}\rangle$, which may cause even higher uncertainties, and an increased sensitivity [6].

V. Recognizing and Reducing the Effect of Noise in the Two-Antenna Method

If one does not know the expected efficiency of the antenna under test (AUT), it can be hard to tell whether or not the two-antenna method efficiency estimate is affected by noise, since S_{11} can have a high SNR, while $S_{11,s}$ may not. An intuitive approach to uncover the noise effect is by investigating the estimated e_b. It is valuable to know that the physical e_b should be between approximately two and four for lower frequency bands [46], [56], but since the calculation of the estimate directly depends on $S_{ii,s}$ as well (see equation (25) in [32]), the calculated estimate can deviate significantly further from those values. Therefore, observing a significant difference between the expected physical e_b and the calculated estimate can be an indicator of the noise effect. Fig. 5 shows e_b for Use Case 3, calculated between Antenna 1 and 2, measured with different signal powers. For all frequencies, the e_b estimate is much higher than usual and, therefore, this measurement is likely significantly affected by noise. Note that increasing the VNA output power and, hence, increasing SNR if the signal source noise is not dominant, reduces e_b (see Fig. 5). Reducing the IF bandwidth can also increase SNR but at the cost of increased measurement time.

One can also perform one two-antenna-method measurement with two broadband and high-total-efficiency antennas and then, perform the same measurement again after replacing one of the antennas with the AUT. If the efficiency estimate of the broadband, high-total-efficiency antenna that was present in both measurements is significantly different between the

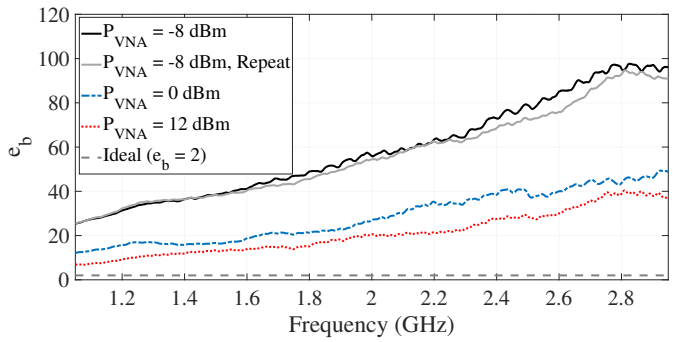

Fig. 5. Enhanced backscatter constant for 2 repeats with VNA signal power -8 dBm, and one repeat with a 12 dBm signal power, compared to the ideal value of $e_b = 2$, as it would be in the one-antenna method. e_b relies directly on $S_{11,s}$ and is therefore overestimated as well. For increased signal powers, hence higher SNRs, the e_b estimate gets closer to a realistic value (approximately 2).

measurements, it is likely that the estimate of the AUT is also not correct due to a low SNR.

Other indicators of the noise effects are an increased uncertainty over position (as explained in Section IV-C-2) and an S_{11} variance that is in the same order of the S_{21} variance (when Antenna 1 has a much lower efficiency, the former should be much smaller). These effects should all reduce when signal power is increased. We are currently researching modeling and measurement methods to develop a noise correction factor for cases where increasing signal power is not a possibility [39]. Note that the modified two-antenna technique proposed in [31] was less susceptible to noise effects, since it removed the dependency on $\langle|S_{11,s}|^2\rangle$, but at a cost of additional assumptions from the one-antenna method.

It should be noted that the noise effects vary significantly for different chambers and antenna set-ups, but they also vary for different antennas. A chamber with high losses or a VNA with a lower dynamic range may show the noise effect more significantly. The effect of the chamber is clearly shown in the differences between the antenna efficiency estimates of Fig. 1 and Fig. 4, where the setup was the same, but a different chamber was used. Besides that, the noise effect described in this work does not just affect the antenna efficiency estimate. Other metrics, such as the chamber transfer function, Total Radiated Power (TRP) and Total Isotropic Sensitivity (TIS) are dependent on antenna efficiency and the variance of S-parameters. This may cause significant errors and uncertainties in the estimates of such metrics.

VI. Conclusion

In this paper, we have shown that discrepancies and increased uncertainties can arise in the measurement-based estimate of antenna efficiency with the two-antenna method when high-loss or highly-mismatched antennas are used. In such cases, the contribution of noise to the estimated S-parameter variance can become higher than the contribution from the paddles, leading to an overestimation of the stirred-energy component and, therefore, the variance. We showed that, for antennas with a low total efficiency, the variance of the measured reflection parameters is more sensitive to noise than the variance of the transmission parameters due to a much lower stirred component. Therefore this effect is more significant in the one- and two-antenna methods, due to their dependency on such parameters, as compared to the three-antenna method total-efficiency estimate, which does not depend on reflection parameters. In the two-antenna method, noise effects can be recognized by an overestimated enhanced backscattering constant, underestimated efficiency of the reference antenna, and uncertainties that are much higher than usual. These effects are highly dependent on VNA settings, chamber setup and the type of antenna. In general, we have shown they may be reduced by increasing signal power. Future research will investigate techniques which can correct for these noise effects.

Acknowledgements

The authors would like to thank NIST colleagues John Ladbury, Benjamin Jamroz and Robert D. Horansky for useful discussions and Christopher L. Holloway and Daniel Kuester for their thorough review of this manuscript.

References

[1] "On the pulse of the networked society," *Ericsson Mobility Report*, 2019. [Online]. Available: https://www.ericsson.com/4acd7e/assets/local/mobility-report/documents/2019/emr-november-2019.pdf

[2] J. G. Andrews, S. Buzzi, W. Choi, S. V. Hanly, A. Lozano, A. C. K. Soong, and J. C. Zhang, "What will 5G be?" *IEEE Journal on Selected Areas in Communications*, vol. 32, no. 6, pp. 1065–1082, Jun 2014.

[3] A. Ghosh, A. Maeder, M. Baker, and D. Chandramouli, "5G evolution: A view on 5G cellular technology beyond 3gpp release 15," *IEEE Access*, vol. 7, pp. 127 639–127 651, 2019.

[4] D. Liu, W. Hong, T. S. Rappaport, C. Luxey, and W. Hong, "What will 5G antennas and propagation be?" *IEEE Transactions on Antennas and Propagation*, vol. 65, no. 12, pp. 6205–6212, Dec 2017.

[5] K. A. Remley, J. A. Gordon, D. Novotny, A. E. Curtin, C. L. Holloway, M. T. Simons, R. D. Horansky, M. S. Allman, D. Senic, M. Becker, J. A. Jargon, P. D. Hale, D. F. Williams, A. Feldman, J. Cheron, R. Chamberlin, C. Gentile, J. Senic, R. Sun, P. B. Papazian, J. Quimby, M. Mujumdar, and N. Golmie, "Measurement challenges for 5G and beyond: An update from the National Institute of Standards and Technology," *IEEE Microwave Magazine*, vol. 18, no. 5, pp. 41–56, Jul 2017.

[6] L. A. Bronckers, A. Roc'h, and A. B. Smolders, "A new design method for frequency- reconfigurable antennas using multiple tuning components," *IEEE Transactions on Antennas and Propagation*, vol. 67, no. 12, pp. 7285–7295, Dec 2019.

[7] S. M. Abbas, Y. Ranga, A. K. Verma, and K. P. Esselle, "A simple ultra wideband printed monopole antenna with high band rejection and wide radiation patterns," *IEEE Transactions on Antennas and Propagation*, vol. 62, no. 9, pp. 4816–4820, Sep 2014.

[8] J. Xu, D. Shen, X. Zhang, and K. Wu, "A compact disc ultrawideband (UWB) antenna with quintuple band rejections," *IEEE Antennas and Wireless Propagation Letters*, vol. 11, pp. 1517–1520, 2012.

[9] J. Jang and H. Hwang, "An improved band-rejection UWB antenna with resonant patches and a slot," *IEEE Antennas and Wireless Propagation Letters*, vol. 8, pp. 299–302, 2009.

[10] R. K. Singh, A. Basu, and S. K. Koul, "A novel reconfigurable microstrip patch antenna with polarization agility in two switchable frequency bands," *IEEE Transactions on Antennas and Propagation*, vol. 66, no. 10, pp. 5608–5613, Oct 2018.

[11] M. Ikram, E. A. Abbas, N. Nguyen-Trong, K. H. Sayidmarie, and A. Abbosh, "Integrated frequency-reconfigurable slot antenna and connected slot antenna array for 5G and 5G mobile handsets," *IEEE Transactions on Antennas and Propagation*, vol. 67, no. 12, pp. 7225–7233, Dec 2019.

[12] K. Alqurashi, J. R. Kelly, Z. Wang, C. Crean, R. Mittra, M. Khalily, and Y. Gao, "Liquid metal bandwidth reconfigurable antenna," *IEEE Antennas and Wireless Propagation Letters*, pp. 1–1, 2019.

[13] C. Mao, S. Gao, Y. Wang, Y. Liu, X. Yang, Z. Cheng, and Y. Geng, "Integrated dual-band filtering/duplexing antennas," *IEEE Access*, vol. 6, pp. 8403–8411, 2018.

[14] Y. Chun, J. Hong, P. Bao, T. J. Jackson, and M. J. Lancaster, "Tunable slotted ground structured bandstop filter with bst varactors," *IET Microwaves, Antennas Propagation*, vol. 3, no. 5, pp. 870–876, Aug 2009.

[15] Kyungho Chung, Jaemoung Kim, and Jaehoon Choi, "Wideband microstrip-fed monopole antenna having frequency band-notch function," *IEEE Microwave and Wireless Components Letters*, vol. 15, no. 11, pp. 766–768, Nov 2005.

[16] T. Ma and J. Tsai, "Band-rejected ultrawideband planar monopole antenna with high frequency selectivity and controllable bandwidth using inductively coupled resonator pairs," *IEEE Transactions on Antennas and Propagation*, vol. 58, no. 8, pp. 2747–2752, Aug 2010.

[17] H. Liu, C. Ku, T. Wang, and C. Yang, "Compact monopole antenna with band-notched characteristic for UWB applications," *IEEE Antennas and Wireless Propagation Letters*, vol. 9, pp. 397–400, 2010.

[18] J. Perruisseau-Carrier, P. Pardo-Carrera, and P. Miskovsky, "Modeling, design and characterization of a very wideband slot antenna with reconfigurable band rejection," *IEEE Transactions on Antennas and Propagation*, vol. 58, no. 7, pp. 2218–2226, Jul 2010.

[19] H. A. Majid, M. K. A. Rahim, M. R. Hamid, and M. F. Ismail, "A compact frequency-reconfigurable narrowband microstrip slot antenna," *IEEE Antennas and Wireless Propagation Letters*, vol. 11, pp. 616–619, 2012.

[20] C. Balanis, *Antenna Theory Analysis and Design*. John Wiley & Sons, New York, 1997, vol. 2.

[21] Q. Xu and Y. Huang, "Inter-comparison between antenna radiation efficiency measurements performed in an anechoic chamber and in a reverberation chamber," in *Anechoic and Reverberation Chambers: Theory, Design, and Measurements*. IEEE, 2018, pp. 305–321.

[22] D. M. Pozar and B. Kaufman, "Comparison of three methods for the measurement of printed antenna efficiency," *IEEE Transactions on Antennas and Propagation*, vol. 36, no. 1, pp. 136–139, Jan 1988.

[23] N. Serafimov, P. . Kildal, and T. Bolin, "Comparison between radiation efficiencies of phone antennas and radiated power of mobile phones measured in anechoic chambers and reverberation chamber," in *IEEE Antennas and Propagation Society International Symposium (IEEE Cat. No.02CH37313)*, vol. 2, 2002, pp. 478–481 vol.2.

[24] A. Diallo, C. Luxey, G. Kossiavas, P. Besnier, A. Chousseaud, Y. Mahe, S. Toutain, B. Derat, C. Delaveaud, L. Robert, J. Carlsson, P. Kildal, C. Orlenius, and O. Litschke, "Comparison of efficiency measurement methods for small antennas," in *11th International Symposium on Antenna Technology and Applied Electromagnetics [ANTEM 2005]*, 2005, pp. 1–4.

[25] P. Kildal, X. Chen, C. Orlenius, M. Franzen, and C. S. L. Patane, "Characterization of reverberation chambers for ota measurements of wireless devices: Physical formulations of channel matrix and new uncertainty formula," *IEEE Transactions on Antennas and Propagation*, vol. 60, no. 8, pp. 3875–3891, 2012.

[26] C. S. Lee, A. Duffy, and C. Lee, "Antenna efficiency measurements in a reverberation chamber without the need for a reference antenna," *IEEE Antennas and Wireless Propagation Letters*, vol. 7, pp. 448–450, 2008.

[27] A. Khaleghi, "Time-domain measurement of antenna efficiency in reverberation chamber," *IEEE Transactions on Antennas and Propagation*, vol. 57, no. 3, pp. 817–821, Mar 2009.

[28] H. G. Krauthäuser and M. Herbrig, "Yet another antenna efficiency measurement method in reverberation chambers," in *2010 IEEE International Symposium on Electromagnetic Compatibility*, Jul 2010, pp. 536–540.

[29] A. Gifuni, I. D. Flintoft, S. J. Bale, G. C. R. Melia, and A. C. Marvin, "A theory of alternative methods for measurements of absorption cross section and antenna radiation efficiency using nested and contiguous reverberation chambers," *IEEE Transactions on Electromagnetic Compatibility*, vol. 58, no. 3, pp. 678–685, Jun 2016.

[30] IEC, "61000-4-21: EMC part 4: Testing and measurement techniques; section 21: Reverberation chamber test methods," 2001.

[31] Q. Xu, Y. Huang, X. Zhu, L. Xing, Z. Tian, and C. Song, "A modified two-antenna method to measure the radiation efficiency of antennas in a reverberation chamber," *IEEE Antennas and Wireless Propagation Letters*, vol. 15, pp. 336–339, 2016.

[32] C. L. Holloway, H. A. Shah, R. J. Pirkl, W. F. Young, D. A. Hill, and J. Ladbury, "Reverberation chamber techniques for determining the radiation and total efficiency of antennas," *IEEE Transactions on Antennas and Propagation*, vol. 60, no. 4, pp. 1758–1770, Apr 2012.

[33] J. B. Coder, J. M. Ladbury, and M. Gołkowski, "A two-port model for antennas in a reverberation chamber," *IEEE Transactions on Antennas and Propagation*, vol. 62, no. 5, pp. 2338–2350, 2014.

[34] C. L. Holloway, H. A. Shah, R. J. Pirkl, K. A. Remley, D. A. Hill, and J. Ladbury, "Early time behavior in reverberation chambers and its effect on the relationships between coherence bandwidth, chamber decay time, rms delay spread, and the chamber buildup time," *IEEE Transactions on Electromagnetic Compatibility*, vol. 54, no. 4, pp. 714–725, Aug 2012.

[35] L. A. Bronckers, A. Roc'h, and A. B. Smolders, "Chasing the wave in a reverberation chamber," in *2018 International Symposium on Electromagnetic Compatibility (EMC EUROPE)*, Aug 2018, pp. 708–712.

[36] C. L. Holloway, R. S. Smith, C. R. Dunlap, R. J. Pirkl, J. Ladbury, W. F. Young, D. A. Hill, W. R. Hansell, M. A. Shadish, and K. B. Sullivan, "Validation of a two-antenna reverberation-chamber technique for estimating the total and radiation efficiency of antennas," in *International Symposium on Electromagnetic Compatibility - EMC EUROPE*, Sep 2012, pp. 1–6.

[37] C. L. Holloway, H. A. Shah, R. Pirkl, W. F. Young, D. A. Hill, and J. Ladbury, "A three-antenna technique for determining the total and radiation efficiencies of antennas in reverberation chambers," *IEEE Antennas and Propagation Magazine*, vol. 54, no. 1, pp. 235–241, Feb 2012.

[38] S. O. Rice, "Mathematical analysis of random noise," *The Bell System Technical Journal*, vol. 23, no. 3, pp. 282–332, 1944.

[39] D. Gu, J. A. Jargon, M. J. Ryan, and A. Hubrechsen, "Influence of noise on scattering-parameter measurements," *IEEE Transactions on Microwave Theory and Techniques*, vol. 68, no. 11, pp. 4925–4939, 2020.

[40] IEEE Std 145-1993(R2004), "IEEE standard definitions of terms for antennas," September 2004.

[41] D. A. Hill, *Electromagnetic Fields in Cavities: Deterministic and Statistical Theories*. Piscataway, NJ, USA: Wiley-IEEE Press, 2009.

[42] K. A. Remley, J. Dortmans, C. Weldon, R. D. Horansky, T. B. Meurs, C. Wang, D. F. Williams, C. L. Holloway, and P. F. Wilson, "Configuring and verifying reverberation chambers for testing cellular wireless devices," *IEEE Transactions on Electromagnetic Compatibility*, vol. 58, no. 3, pp. 661–672, Jun 2016.

[43] J. C. West, J. N. Dixon, N. Nourshamsi, D. K. Das, and C. F. Bunting, "Best practices in measuring the quality factor of a reverberation chamber," *IEEE Transactions on Electromagnetic Compatibility*, vol. 60, no. 3, pp. 564–571, Jun 2018.

[44] X. Zhang, M. P. Robinson, I. D. Flintoft, and J. F. Dawson, "Efficient determination of reverberation chamber time constant," *IEEE Transactions on Electromagnetic Compatibility*, vol. 60, no. 5, pp. 1296–1303, Oct 2018.

[45] J. Ladbury and D. A. Hill, "Enhanced backscatter in a reverberation chamber: Inside every complex problem is a simple solution struggling to get out," in *2007 IEEE International Symposium on Electromagnetic Compatibility*, Jul 2007, pp. 1–5.

[46] L. A. Bronckers, A. Roc'h, and A. B. Smolders, "Reverberation chamber enhanced backscattering: High-frequency effects," in *2019 International Symposium on Electromagnetic Compatibility - EMC EUROPE*, Sep 2019, pp. 1–6.

[47] G. Lerideau, E. Amador, P. Besnier, and C. Lemoine, "Quantifying stirred and unstirred components in reverberation chamber with appropriate statistics," in *2009 IEEE International Symposium on Electromagnetic Compatibility*, Aug 2009, pp. 182–186.

[48] L. A. Bronckers, K. A. Remley, B. F. Jamroz, A. Roc'h, and A. Bart Smolders, "Uncertainty in reverberation-chamber antenna-efficiency measurements in the presence of a phantom," *IEEE Transactions on Antennas and Propagation*, vol. 68, no. 6, pp. 4904–4915, 2020.

[49] D. F. Williams, "NIST microwave uncertainty framework, version 1.4.26.24158, National Institute of Standards and Technology," 2019.

[50] J. A. Jargon, D. F. Williams, A. C. Stelson, C. J. Long, A. M. Hagerstrom, P. D. Hale, J. R. Stoup, E. S. Stanfield, W. Ren, "Physical models and dimensional traceability of WR15 rectangular waveguide standards for determining systematic uncertainties of calibrated scattering-parameters," National Institute of Standards and Technology, Tech. Rep., 2020, technical note (NIST TN) - 2109.

[51] G. Avolio, D. F. Williams, S. Streett, M. Frey, D. Schreurs, A. Ferrero, and M. Dieudonné, "Software tools for uncertainty evaluation in vna measurements: A comparative study," in *2017 89th ARFTG Microwave Measurement Conference (ARFTG)*, 2017, pp. 1–7.

[52] J. A. Jargon, D. F. Williams, and P. D. Hale, "Developing models for type-n coaxial vna calibration kits within the nist microwave uncertainty

framework," in *2016 87th ARFTG Microwave Measurement Conference (ARFTG)*, 2016, pp. 1–4.
[53] B. F. Jamroz and D. F. Williams, "Consistency in monte carlo uncertainty analyses," *Metrologia*, vol. 57, no. 6, p. 065008, oct 2020. [Online]. Available: https://doi.org/10.1088/1681-7575/aba5aa
[54] Joint Committee for Guides in Metrology. (2008, Sep.). Evaluation of Measurement Data—Guide to the Expression of Uncertainty in Measurement. Intl. Bureau Weights Measures, Sevres, France ' [Online]. Available: http://www.bipm.org/en/publications/guides/gum.html.
[55] J. A. Jargon, D. F. Williams, and A. Sanders, "The relationship between switch-term-corrected scattering-parameters and wave-parameters measured with a two-port vector network analyzer," *IEEE Microwave and Wireless Components Letters*, vol. 28, no. 10, pp. 951–953, 2018.
[56] Zhihao Tian, Yi Huang, and Qian Xu, "Enhanced backscatter coefficient measurement at high frequencies in reverberation chamber," in *2017 International Workshop on Electromagnetics: Applications and Student Innovation Competition*, May 2017, pp. 166–167.

Anouk Hubrechsen received the B.Sc. and M.Sc. degrees in electrical engineering from the Eindhoven University of Technology, Eindhoven, The Netherlands, in 2017 and 2019, respectively, where she is currently pursuing the Ph.D. degree.

She was a Guest Researcher with the National Institute of Standards and Technology, Boulder, CO, USA, in 2019, where she was involved in reverberation-chamber metrology for Internet-of-Things applications. She is currently involved in a project on reverberation-chamber technology for 5G-and-beyond mm-wave applications. Ms. Hubrechsen received the regional and district Zonta Women in Technology awards in 2019. From 2020 to 2021, she was vice-chair of IEEE Benelux Women in Engineering.

Kate A. Remley (S'92-M'99-SM'06-F'13) was born in Ann Arbor, MI. She received the Ph.D. degree in Electrical and Computer Engineering from Oregon State University, Corvallis, in 1999.

From 1983 to 1992, she was a Broadcast Engineer in Eugene, OR, serving as Chief Engineer of an AM/FM broadcast station from 1989-1991. In 1999, she joined the RF Technology Division of the National Institute of Standards and Technology (NIST), Boulder, CO, as an Electronics Engineer. She is currently the Leader of the Metrology for Wireless Systems Project at NIST, where her research activities include development of calibrated measurements for microwave and millimeter-wave wireless systems and standardized over-the-air test methods for the wireless industry.

Dr. Remley is a Fellow of the IEEE and was the recipient of the Department of Commerce Bronze and Silver Medals, an Automatic RF Techniques Group (ARFTG) Best Paper Award, the NIST Schlichter Award, and is a member of the Oregon State University Academy of Distinguished Engineers. She was the Chair of the MTT-11 Technical Committee on Microwave Measurements (2008-2010), the Editor-in-Chief of IEEE Microwave Magazine (2009-2011), and Chair of the MTT Fellow Evaluating Committee (2017-2018). She was a Distinguished Lecturer for the IEEE Electromagnetic Compatibility Society (2016-2017).

Robert Jones received dual B.S. degrees in electrical and mechanical engineering from the Colorado School of Mines (Golden, Colorado, USA) in 2019, where he is currently pursuing his masters degree. Since 2017, he has been a student researcher at the National Institute of Standards and Technology (NIST), conducting experiments with loaded reverberation chambers.

His current research interests are in computational electromagnetics, antenna design, and loaded reverberation chamber metrology.

Dylan F. Williams (M'80-SM'90-F'02) received a Ph.D. in Electrical Engineering from the University of California, Berkeley in 1986. He joined the Electromagnetic Fields Division of the National Institute of Standards and Technology in 1989 where he develops electrical waveform and microwave metrology. He has published over 140 technical papers and is a Fellow of the IEEE. He is the recipient of the Department of Commerce Bronze and Silver Medals, the Astin Measurement Science Award, two Electrical Engineering Laboratory's Outstanding Paper Awards, three Automatic RF Techniques Group (ARFTG) Best Paper Awards, the ARFTG Automated Measurements Technology Award, the IEEE Morris E. Leeds Award, the European Microwave Prize and the 2013 IEEE Joseph F. Keithley Award. Dylan also served as Editor of the IEEE Transactions on Microwave Theory and Techniques from 2006 to 2010, as the Executive Editor of the IEEE Transactions on Terahertz Science and Technology, and as the 2017 President of the IEEE Microwave Theory and Techniques Society.

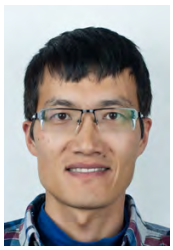

Dazhen Gu received the Ph.D. degree in electrical engineering from University of Massachusetts, Amherst, in 2007.

He has been with the RF Technology Division, National Institute of Standards and Technology (NIST), Boulder, CO, since November 2003. During the first three and a half years, he did his doctoral research in development of terahertz imaging components and systems. From 2007 to 2009, he was with the Microwave Measurement Services project, where he was involved in microwave metrology, in particular thermal noise measurements and instrumentation. From 2009 to 2015, he took a position in the microwave remote-sensing project, in which a microwave brightness-temperature standard was successfully demonstrated. From 2015 to 2018, he was in charge of the microwave power project and developed the NIST power traceability with correlated uncertainties for 5G communication researches. Since March 2018, he has been with the Shared-Spectrum Metrology Group, where he is involved in the Spectrum Sensing and Noise Project

Bart Smolders was born in Hilvarenbeek, the Netherlands in 1965. He received his M.Sc. and Ph.D. degree in Electrical Engineering from the Eindhoven University of Technology (TU/e) in 1989 and 1994, respectively. From 1989 to 1991, he worked as an IC Designer at FEL-TNO, The Hague. From 1994 to 1997, he was a Radar System Designer with Thales, the Netherlands. From 1997 to 2000, he was project leader of the Square Kilometer Array (SKA) with the Netherlands Foundation for Research in Astronomy (ASTRON). From 2000 to 2010, he has been with NXP (formerly Philips) Semiconductors, The Netherlands, responsible for the innovation in the RF business line. Since 2010, he is a full-time professor at the TU/e in the Electromagnetics Group with special interest in antenna systems and applications. He currently leads several research projects in the area of integrated antenna systems operating at frequencies up to 150 GHz for several application domains, including 5G/6G wireless communications, radar sensors and radio-astronomy. He is junior-past chairman of the IEEE Benelux section and past-chair of the NERG (Nederlands Radio- en Elektronica Genootschap). He is Board member of the SWAN (Stichting Wetenschappelijke Activiteiten van het Nederlands URSI Committee) and member of the Advisory Board of ASTRON and PhotonDelta. Next to his research activities, he is the dean of the Electrical Engineering department of the TU/e. He has published more than 150 papers. More details can be found at: https://www.tue.nl/en/research/researchers/bart-smolders/

Laurens A. Bronckers received the M.Sc. degree (cum laude) in electrical engineering from Eindhoven University of Technology (TU/e), The Netherlands, in 2015. In 2018, he was a visiting researcher at The National Institute of Standards and Technology (NIST) in Boulder, Colorado, on antenna measurements in reverberation chambers. He obtained the Ph.D. degree (cum laude) in electrical engineering in 2019, within the electromagnetics group at TU/e, on design and measurement techniques for next-generation integrated antennas. He is currently an assistant professor on Metrology for Antennas and Wireless Systems at TU/e. His research interests include antenna measurements in reverberation and anechoic chambers, channel sounding and emulation, and RF material characterization.